The *ab initio* ground state properties and magnetic structure of plutonium

The *ab initio* ground state properties and magnetic structure of plutonium

A L Kutepov and S G Kutepova[1]

Institute of Technical Physics, PO Box 245, 456770 Snezhinsk, Chelyabinsk Region, Russia

E-mail: A.L.Kutepov@vniitf.ru

Abstract
Using the fully relativistic, full potential, spin-polarized, linearized augmented-plane-wave (RSPFLAPW) method, the energy differences, the electronic structure and magnetic moments of alpha- and delta-plutonium with different alignments of the atomic magnetic moments have been calculated. We have found in our calculations that both α-Pu and δ-Pu structures have an antiferromagnetic order at their experimental equilibrium volumes. Similar results have also been obtained by other researchers for δ-Pu. An important conclusion from the present work is that taking the spin polarization into account improves the calculated density of states for α-Pu. This fact may be considered as an argument for the importance of magnetic interactions in the low temperature phase of plutonium.

1. Introduction

In accordance with 5f electron behaviour, actinides can be divided into two groups [1]. The character of 5f electrons in the light actinides from Th to Np is almost purely metallic. But the nature of the bonding changes dramatically with Am, whose 5f electrons are localized, and the volumes of Am, Cm, Bk, and Cf at $T = 0$ are about 50% larger than that of Np. Plutonium lies between these two groups of actinides. Thus, to understand the competition between localization and delocalization of 5f electrons, Pu is a crucial element.

The electronic structure and the ground state properties of the given actinide element have been studied extensively over the years [2–22]. The principal conclusion obtained from these investigations is that correlation effects are very important for high temperature phases of Pu and that the standard density functional theory (DFT) (local density approximation, LDA, or generalized gradient approximation, GGA) is inadequate for the description of some anomalous properties of them. In fact, in the calculations performed within the LDA, the equilibrium volume of δ-Pu has been underestimated (up to 30%) and the calculated bulk modulus is

---

[1] Author to whom any correspondence should be addressed.

about four times larger [6, 13]. GGA does not change the situation considerably [6, 13]. The equilibrium volume of δ-Pu has been reproduced by Penicaud [17] via cancelling the coupling between $5f_{5/2}$ and s, p, d electrons, and via reducing the coupling between $5f_{5/2}$ and $5f_{7/2}$ electrons. In addition, Savrasov and Kotliar [12] have shown that the rather unusual atomic volume of δ-Pu may be described within the GGA + U method using the Hubbard parameter, U, equal to 4 eV. Recently, the first attempt has been undertaken by Savrasov *et al* [19] to describe the correlated electrons in δ-Pu within a dynamical mean-field theory (DMFT). With the Coulomb repulsion energy U also equal to 4 eV, they were able to reproduce the experimental equilibrium volume of δ-Pu.

However, there are some results of another kind. Wang and Sun [14] have reproduced well the ground state properties of δ-Pu and ϵ-Pu within the usual spin-polarized GGA and with antiferromagnetic (AFM) configurations. In addition, rather interesting results have been obtained by Söderlind [20], who has studied the structural and magnetic properties of some of the phases of plutonium. The principal conclusion of Söderlind's work on δ-Pu was the same as in [14]: a magnetic structure with AFM ordering has the lowest energy, and the ground state properties of this phase of Pu are reproduced well, within the spin-polarized GGA. This conclusion is very important because Curie–Weiss behaviour has been found in δ-Pu magnetic susceptibility at high temperatures [23], although magnetic ordering has not been observed at low temperatures, in [23] (supposedly via a Kondo-type effect). Apart from that, in the recent work by Söderlind *et al* [22], the high temperature disorder in δ-Pu has also been modelled with some success within the spin-polarized GGA. Thus, there are reasons to believe that in δ-Pu local magnetic moments are formed, and this fact may be described within the standard spin-polarized GGA. This does not exclude, however, the necessity for a many-particle theory for a complete description of the whole spectrum of anomalous properties of this phase of Pu.

The situation with α-Pu is also unresolved. Traditionally, the alpha phase is regarded as well understood within the non-spin-polarized GGA [20]. However, we believe that the situation is not so simple. Indeed, recent DMFT calculations [19] indicate the presence of correlations in α-Pu. We also think that the magnetic interactions play some role in forming the electronic structure of this plutonium phase, although there is no direct experimental evidence of magnetic moments in α-Pu. However, support for magnetic interactions first comes from an anomalous temperature dependence of plutonium's electrical resistivity [24], which has been explained by Jullien *et al* [25] as enhanced electron scattering that results from the spin fluctuations. Secondly, support comes from experiments on magnetic susceptibility [23]. The magnetic susceptibility of α-Pu is lower than that of materials with local moments, but it is higher than that of most metals. It is essentially temperature independent at $T > 40$ K, but below 40 K susceptibility becomes strongly temperature dependent, although experimental uncertainties are large in the low temperature range. It is interesting that the temperature dependence of magnetic susceptibility has been observed in the same range of temperatures in which the slope of temperature dependence for the electrical resistivity is highest. In addition, a comparison of the light actinides with the transition metals indicates that the light actinides should be superconductors unless they have some magnetic structure. The fact that Pu is not a superconductor may indicate that plutonium is an incipient, weak itinerant magnet [26].

The idea that taking the spin polarization into account is important also arises because the non-spin-polarized calculations [13, 20, 21] underestimate the equilibrium volume in comparison with the experimental volume and overestimate considerably the calculated bulk modulus (up to three times, see table 4). Spin-polarized calculations were first carried out some time ago. Antropov *et al* [7] performed the spin-polarized calculations on α-Pu and found that the ground state of this plutonium phase is a compensated antiferromagnet. Unfortunately, these authors did not calculate the ground state properties. Also, they did not use a full-potential

code and hence their results are doubtful. On the other hand, Söderlind [20] found from his spin-polarized calculations that α-Pu is non-magnetic (NM) at the experimental equilibrium volume. However, some simplifications were also made in his calculations. The spin–orbit interaction has been treated as a variational step and the Gaussian broadening of electronic states in the Brillouin zone (BZ) integrations might be a reason for suppressing the magnetic moments. In any case, there is no full understanding of magnetism in α-Pu.

The present paper is devoted to a theoretical study of the energy differences, the electronic and magnetic structures of α-Pu and δ-Pu. For δ-Pu we have examined whether or not the fully relativistic calculations change the conclusions about the antiferromagnetic ground state. For α-Pu we have studied the possibility of magnetic ordering and the influence of taking the spin polarization and the spin–orbit interaction into account in the calculated electronic structure and in the ground state properties of this phase.

This paper is organized as follows. In section 2 we present our method. The calculation parameters and results are presented in section 3. Lastly, in section 4 we offer our conclusions.

2. The method of calculation

2.1. Relativistic spin-polarized theory

The DFT in the generalized gradient approximation [27] was used in this work. The calculations were performed on the full potential, Dirac relativistic (j, κ) basis, spin-polarized linearized augmented-plane-wave method (RSPFLAPW + LO)². Local orbitals (LO) [28] were added to the basis. Scalar-relativistic calculations were also performed for the purpose of testing the code and studying the influence of taking the spin–orbit interaction into consideration. The employed technique is standard in the case of non-relativistic or scalar-relativistic calculations. Only some detail of the realization of the fully relativistic approach is therefore given below.

The well known approach for a joint description of relativistic and magnetic effects, offered in [29–32], has been adopted. In this approach, the total energy of the system with density n and magnetization m has the form:

$$E[n, m] = T_s[n] + \int_\Omega \mathrm{d}r\, [n(r)V_{ext}(r) + m(r) \cdot B_{ext}(r)]$$
$$+ \int_\Omega \mathrm{d}r \int_\Omega \mathrm{d}r'\, \frac{n(r)n(r')}{|r - r'|} + E_{xc}[n, m] + E_{nn}, \tag{1}$$

where Ω is the volume of the unit cell of a given solid, and we use atomic Rydberg units throughout. $T_s[n]$ is the kinetic energy for the non-interacting single-particle system, defined by

$$T_s[n] = \sum_k \sum_\lambda \int_\Omega \mathrm{d}r\, \Psi_\lambda^\dagger(k, r)\hat{H}_{kin}\Psi_\lambda(k, r)\theta[E_F - E_\lambda(k)], \tag{2}$$

using the Dirac kinetic Hamiltonian $\hat{H}_{kin}$,

$$\hat{H}_{kin} = c\alpha \cdot p + (\beta - I)\frac{c^2}{2}, \tag{3}$$

where c is the velocity of light ($c = 274.074$ in Rydberg units), p is the momentum operator ($\equiv -i\nabla$), and the three operators α, β and I denote the standard Dirac 4×4 matrices. $\Psi_\lambda(k, r)$

---

² All calculations presented in this paper were performed using a computer code written by the authors. Non-relativistic and scalar-relativistic variants of the FLAPW method were coded in close accordance with that given in [28]. The basic formulae of the relativistic variant are given in the text of this paper.

denotes the Bloch function labelled by the band index λ and the reciprocal vector $\boldsymbol{k}$ in the first BZ. $E_\lambda(\boldsymbol{k})$ indicates the band energy, and $\theta(x)$ represents the unit theta function, ensuring that all occupied states with energy less than E_F are included in the sum of equation (2). The charge densities, $n(\boldsymbol{r})$, and the magnetization, $\boldsymbol{m}(\boldsymbol{r})$, are defined using the Bloch function $\Psi_\lambda(\boldsymbol{k}, \boldsymbol{r})$ by

$$n(\boldsymbol{r}) = \sum_{\boldsymbol{k}} \sum_{\lambda} \Psi_\lambda^\dagger(\boldsymbol{k}, \boldsymbol{r}) \Psi_\lambda(\boldsymbol{k}, \boldsymbol{r}) \theta[E_F - E_\lambda(\boldsymbol{k})], \tag{4}$$

and

$$\boldsymbol{m}(\boldsymbol{r}) = \sum_{\boldsymbol{k}} \sum_{\lambda} \Psi_\lambda^\dagger(\boldsymbol{k}, \boldsymbol{r}) \beta \tilde{\boldsymbol{\sigma}} \Psi_\lambda(\boldsymbol{k}, \boldsymbol{r}) \theta[E_F - E_\lambda(\boldsymbol{k})], \tag{5}$$

respectively. Here, $\tilde{\boldsymbol{\sigma}}$ denotes the 4×4 matrices, which is composed of the Pauli matrices $\boldsymbol{\sigma}$ as

$$\tilde{\sigma} = \begin{pmatrix} \sigma & 0 \\ 0 & \sigma \end{pmatrix}. \tag{6}$$

The second term in the right-hand side of (1) gives an external contribution to the total energy, thus the term $V_{ext}(\boldsymbol{r})$ designates a scalar external potential, and $\boldsymbol{B}_{ext}(\boldsymbol{r})$ denotes an external magnetic field. The third term is the classical Coulomb energy, the term E_{xc} gives the exchange and correlation energy, which is a functional of $n(\boldsymbol{r})$ and $\boldsymbol{m}(\boldsymbol{r})$, and the last term E_{nn} is the energy of nuclear–nuclear repulsion.

An application of the Hohenberg–Kohn variational principle [33] to the total energy in (1) leads to a set of self-consistent single-particle equations that enable us to determine the densities, $n(\boldsymbol{r})$, and the magnetization, $\boldsymbol{m}(\boldsymbol{r})$, through equations (4) and (5):

$$\hat{H} \Psi_\lambda(\boldsymbol{k}, \boldsymbol{r}) = E_\lambda(\boldsymbol{k}) \Psi_\lambda(\boldsymbol{k}, \boldsymbol{r}). \tag{7}$$

Here, the spin-polarized Dirac Hamiltonian is given by

$$\hat{H} = \hat{H}_{kin} + V(\boldsymbol{r}) + \beta \tilde{\boldsymbol{\sigma}} \cdot \boldsymbol{B}(\boldsymbol{r}). \tag{8}$$

The scalar effective potential $V(\boldsymbol{r})$ is obtained through the variation as

$$V(\boldsymbol{r}) = V_{ext}(\boldsymbol{r}) + 2 \int_\Omega \mathrm{d}\boldsymbol{r}' \frac{n(\boldsymbol{r}')}{|\boldsymbol{r} - \boldsymbol{r}'|} + \frac{\delta E_{xc}[n(\boldsymbol{r}), \boldsymbol{m}(\boldsymbol{r})]}{\delta n(\boldsymbol{r})}, \tag{9}$$

whereas the effective magnetic field $\boldsymbol{B}(\boldsymbol{r})$ is obtained as

$$\boldsymbol{B}(\boldsymbol{r}) = \boldsymbol{B}_{ext}(\boldsymbol{r}) + \frac{\delta E_{xc}[n(\boldsymbol{r}), \boldsymbol{m}(\boldsymbol{r})]}{\delta \boldsymbol{m}(\boldsymbol{r})}. \tag{10}$$

The kinetic energy (2) can be rewritten using (7), the orthonormality of $\Psi_\lambda(\boldsymbol{k}, \boldsymbol{r})$ and the definitions for $n(\boldsymbol{r})$ and $\boldsymbol{m}(\boldsymbol{r})$:

$$T_s[n] = \sum_c E_c + \sum_{\boldsymbol{k}} \sum_\lambda E_\lambda(\boldsymbol{k}) \theta[E_F - E_\lambda(\boldsymbol{k})] - \int_\Omega \mathrm{d}\boldsymbol{r}\, n(\boldsymbol{r}) V(\boldsymbol{r}) - \int_\Omega \mathrm{d}\boldsymbol{r}\, \boldsymbol{m}(\boldsymbol{r}) \cdot \boldsymbol{B}(\boldsymbol{r}). \tag{11}$$

The first sum represents a core contribution to the eigenvalue sum.

Furthermore, there are three divergent electrostatic contributions in the expression (1) for the total energy. They cancel, however, and after some rearrangements we have:

$$E[n, \boldsymbol{m}] = T_s[n] + \frac{1}{2} \int_\Omega \mathrm{d}\boldsymbol{r}\, n(\boldsymbol{r}) V_C(\boldsymbol{r}) - \frac{1}{2} \sum_a Z_a V_C'(\boldsymbol{t}_a)$$

$$+ \int_\Omega \mathrm{d}\boldsymbol{r}\, \boldsymbol{m}(\boldsymbol{r}) \cdot \boldsymbol{B}_{ext}(\boldsymbol{r}) + E_{xc}[n, \boldsymbol{m}], \tag{12}$$

where vectors $\boldsymbol{t}_a$ represent the atomic positions in the unit cell, Z_a is the nucleus charge on atom a, $V_C(\boldsymbol{r})$ is the Coulomb potential, and $V_C'(\boldsymbol{t}_a)$ is the Coulomb potential at the nucleus without Z_a/r self-contribution.

2.2. Basis functions of the fully relativistic FLAPW + LO method

In the RSPFLAPW method, as in all the APW based schemes, the space in the unit cell is partitioned into MT-spheres Ω_a with radius S_a, surrounding atoms and the interstitial region Ω_i. The scalar potential $V(\boldsymbol{r})$ and magnetic field $\boldsymbol{B}(\boldsymbol{r})$ are decomposed into spherical harmonics inside the MT-spheres. A decomposition into plane waves is used in the interstitial region.

We used basis functions of two types. The basis functions of the first type are characterized by the relativistic plane-wavefunction in the interstitial region:

$$\Phi_A(\boldsymbol{k}+\boldsymbol{G}, s; \boldsymbol{r})|_{\Omega_i} = \frac{N_{\boldsymbol{k}+\boldsymbol{G}}}{\sqrt{\Omega}} \begin{pmatrix} u_s \\ \frac{c\boldsymbol{\sigma}\cdot(\boldsymbol{k}+\boldsymbol{G})}{c^2+\epsilon_{\boldsymbol{k}+\boldsymbol{G}}^+} u_s \end{pmatrix} \exp[i(\boldsymbol{k}+\boldsymbol{G})\cdot\boldsymbol{r}], \tag{13}$$

where $\boldsymbol{G}$ is the reciprocal lattice vector, $\epsilon_{\boldsymbol{k}+\boldsymbol{G}}^+$ is the positive relativistic energy connected with the wavevector $\boldsymbol{k}+\boldsymbol{G}$, i.e., $2\epsilon_{\boldsymbol{k}+\boldsymbol{G}}^+ = -c^2 + c\sqrt{c^2+4(\boldsymbol{k}+\boldsymbol{G})^2}$, $N_{\boldsymbol{k}+\boldsymbol{G}}$, the norm factor, and u_s designates the spinor function for the spin state $s = \pm\frac{1}{2}$.

The basis functions of the second type equal zero in Ω_i.

In the MT-spheres, the basis functions of the first type are constructed from the solutions of the central field Dirac equation with $\boldsymbol{B} = 0$ and with only a spherical component of the effective scalar potential $V_0^a(\boldsymbol{r})$

$$[\hat{H}_{kin} + V_0^a(\boldsymbol{r}) - \epsilon_{il}^a] \begin{pmatrix} g_{il}^a(r) & \Omega_{i;l;\mu} \\ \frac{i}{c} f_{il}^a(r) & \Omega_{-i;l+2i;\mu} \end{pmatrix} = 0 \tag{14}$$

and from their energy derivatives, which are the solutions of the equation

$$[\hat{H}_{kin} + V_0^a(\boldsymbol{r}) - \epsilon_{il}^a] \begin{pmatrix} \dot{g}_{il}^a(r) & \Omega_{i;l;\mu} \\ \frac{i}{c} \dot{f}_{il}^a(r) & \Omega_{-i;l+2i;\mu} \end{pmatrix} = \begin{pmatrix} g_{il}^a(r) & \Omega_{i;l;\mu} \\ \frac{i}{c} f_{il}^a(r) & \Omega_{-i;l+2i;\mu} \end{pmatrix}. \tag{15}$$

In these equations ϵ_{il}^a are the reference energies, which must be determined self-consistently. $\Omega_{i;l;\mu}$ are the spin-angular functions [34]. l is the quantum number of the orbital moment, i determines the total moment j through $j = l + i$ ($i = \pm\frac{1}{2}$, and should not be confused with the imaginary unit i), and μ is the z-projection of the total moment. The relativistic quantum number κ is connected with l and i through

$$\begin{array}{ll} \kappa = l, & i = -\frac{1}{2} \\ \kappa = -l - 1, & i = \frac{1}{2} \end{array}. \tag{16}$$

The spin-angular functions are constructed according to the ordinary scheme of the moments' adding:

$$\Omega_{i;l;\mu} = \sum_{s=\pm\frac{1}{2}} C_{is}^{l\mu} Y_{l;\mu-s}(\hat{\boldsymbol{r}}) u_s, \tag{17}$$

where $Y_{l;\mu-s}(\hat{\boldsymbol{r}})$ are spherical harmonics [35]. $C_{is}^{l;\mu}$ denotes the Clebsch–Gordan coefficient that is easily expressed using the parameter $u_{l\mu} = \mu/(l + 1/2)$ as

$$C^{l;\mu} = \begin{pmatrix} C_{-\frac{1}{2}-\frac{1}{2}}^{l;\mu} & C_{-\frac{1}{2}\frac{1}{2}}^{l;\mu} \\ C_{\frac{1}{2}-\frac{1}{2}}^{l;\mu} & C_{\frac{1}{2}\frac{1}{2}}^{l;\mu} \end{pmatrix} = \frac{1}{\sqrt{2}} \begin{pmatrix} \sqrt{1+u_{l\mu}} & -\sqrt{1-u_{l\mu}} \\ \sqrt{1-u_{l\mu}} & \sqrt{1+u_{l\mu}} \end{pmatrix}. \tag{18}$$

The spin-angular functions are orthonormal, so that

$$\int \Omega_{i;l;\mu}^\dagger \Omega_{i';l';\mu'} \sin\theta \, d\theta \, d\phi = \delta_{ii'}\delta_{ll'}\delta_{\mu\mu'}. \tag{19}$$

The radial functions $g_{il}^a(r)$ and $f_{il}^a(r)$ are the solutions of the following coupled linear differential equations:

$$\frac{d(rg_{il}^a)}{dr} = -\frac{\kappa}{r}(rg_{il}^a) + \frac{c^2 + \epsilon_{il}^a - V_0^a}{c^2}(rf_{il}^a) \tag{20}$$

$$\frac{d(rf_{il}^a)}{dr} = \frac{\kappa}{r}(rf_{il}^a) - (\epsilon_{il}^a - V_0^a)(rg_{il}^a) \tag{21}$$

and for the energy derivatives we have to integrate the following equations:

$$\frac{\mathrm{d}(r\dot{g}_{il}^a)}{\mathrm{d}r} = -\frac{\kappa}{r}(r\dot{g}_{il}^a) + \frac{c^2 + \epsilon_{il}^a - V_0^a}{c^2}(r\dot{f}_{il}^a) + \frac{1}{c^2}(rf_{il}^a) \tag{22}$$

$$\frac{\mathrm{d}(r\dot{f}_{il}^a)}{\mathrm{d}r} = \frac{\kappa}{r}(r\dot{f}_{il}^a) - (\epsilon_{il}^a - V_0^a)(r\dot{g}_{il}^a) - (rg_{il}^a). \tag{23}$$

It is convenient to construct two linear combinations $R_1^{ail\mu}(r)$ and $R_2^{ail\mu}(r)$ from the solutions of (14) and (15):

$$R_1^{ail\mu}(r) = p_1^{ail}\begin{pmatrix} g_{il}^a(r) & \Omega_{i;l;\mu} \\ \frac{\mathrm{i}}{c}f_{il}^a(r) & \Omega_{-i;l+2i;\mu} \end{pmatrix} + q_1^{ail}\begin{pmatrix} \dot{g}_{il}^a(r) & \Omega_{i;l;\mu} \\ \frac{\mathrm{i}}{c}\dot{f}_{il}^a(r) & \Omega_{-i;l+2i;\mu} \end{pmatrix} \tag{24}$$

and

$$R_2^{ail\mu}(r) = p_2^{ail}\begin{pmatrix} g_{il}^a(r) & \Omega_{i;l;\mu} \\ \frac{\mathrm{i}}{c}f_{il}^a(r) & \Omega_{-i;l+2i;\mu} \end{pmatrix} + q_2^{ail}\begin{pmatrix} \dot{g}_{il}^a(r) & \Omega_{i;l;\mu} \\ \frac{\mathrm{i}}{c}\dot{f}_{il}^a(r) & \Omega_{-i;l+2i;\mu} \end{pmatrix} \tag{25}$$

in such a manner that they have the following properties at the boundary of the MT-sphere (S_a):

$$R_1^{ail\mu}(S_a) = \begin{pmatrix} 1 & \Omega_{i;l;\mu} \\ 0 & \Omega_{-i;l+2i;\mu} \end{pmatrix} \tag{26}$$

and

$$R_2^{ail\mu}(S_a) = \begin{pmatrix} 0 & \Omega_{i;l;\mu} \\ \frac{\mathrm{i}}{c}\cdot 1 & \Omega_{-i;l+2i;\mu} \end{pmatrix}. \tag{27}$$

Now we can write down the basis functions of the first type in the MT-spheres as

$$\Phi_A(k+G, s, r)|_{\Omega_a} = \sum_{il\mu}\left[y_1^{ail\mu}(k+G, s)R_1^{ail\mu}(r) + y_2^{ail\mu}(k+G, s)R_2^{ail\mu}(r)\right]. \tag{28}$$

The properties (26), (27) and the requirement of continuity for the large and small components of the functions as defined in (13) and (28) across the boundary of the MT-spheres for all the quantum numbers (i, l, μ) with $l \leqslant l_{max}$ allow us to determine the coefficients $y_1^{ail\mu}(k+G, s)$ and $y_2^{ail\mu}(k+G, s)$:

$$y_1^{ail\mu}(k+G, s) = \frac{4\pi}{\sqrt{\Omega}}\mathrm{i}^l\mathrm{e}^{\mathrm{i}(k+G)t_a}N_{k+G}C_{is}^{l\mu}j_l(|k+G|S_a)Y_{l\mu-s}^*(\widehat{k+G}) \tag{29}$$

$$y_2^{ail\mu}(k+G, s) = \frac{4\pi}{\sqrt{\Omega}}\mathrm{i}^{l-2i}\mathrm{e}^{\mathrm{i}(k+G)t_a}N_{k+G}C_{is}^{l\mu}\frac{c^2|k+G|}{c^2 + \epsilon_{k+G}^+}j_{l+2i}(|k+G|S_a)Y_{l\mu-s}^*(\widehat{k+G}). \tag{30}$$

The basis functions of the second type are the local functions. They are determined only inside the MT-spheres and can be used to enhance the variational freedom of the valence states and allow the semicore orbitals to be treated together with the valence electrons. The construction of the LO is done by starting with the solutions of (14) and (15) at appropriately chosen energy parameters ϵ_n^a, where n designate the set of the quantum numbers that distinguish the local orbitals from one another. Then, the second derivative of the solution of (14) is added, with the particular linear combination R_3^{an} determined by the conditions that the large and small components of it go to zero at the sphere boundary, and choosing the coefficient of the second derivative to be unity:

$$R_3^{an}(r) = p_3^{an}\begin{pmatrix} g_{il}^a(r) & \Omega_{i;l;\mu} \\ \frac{\mathrm{i}}{c}f_{il}^a(r) & \Omega_{-i;l+2i;\mu} \end{pmatrix} + q_3^{an}\begin{pmatrix} \dot{g}_{il}^a(r) & \Omega_{i;l;\mu} \\ \frac{\mathrm{i}}{c}\dot{f}_{il}^a(r) & \Omega_{-i;l+2i;\mu} \end{pmatrix}$$
$$+ \begin{pmatrix} \ddot{g}_{il}^a(r) & \Omega_{i;l;\mu} \\ \frac{\mathrm{i}}{c}\ddot{f}_{il}^a(r) & \Omega_{-i;l+2i;\mu} \end{pmatrix}. \tag{31}$$

The second derivatives are found as the solutions of the equations:

$$[\hat{H}_{kin} + V_0^a(r) - \epsilon_n^a] \begin{pmatrix} \ddot{g}_n^a(r) & \Omega_n^\mu \\ \frac{i}{c} \ddot{f}_n^a(r) & \Omega_{-n\mu} \end{pmatrix} = 2 \begin{pmatrix} \dot{g}_n^a(r) & \Omega_{n\mu} \\ \frac{i}{c} \dot{f}_n^a(r) & \Omega_{-n\mu} \end{pmatrix}, \tag{32}$$

and we have to integrate the following equations for the second energy derivatives of the radial functions:

$$\frac{\mathrm{d}(r\ddot{g}_n^a)}{\mathrm{d}r} = -\frac{\kappa}{r}(r\ddot{g}_n^a) + \frac{c^2 + \epsilon_n^a - V_0^a}{c^2}(r\ddot{f}_n^a) + \frac{2}{c^2}(r\dot{f}_n^a) \tag{33}$$

$$\frac{\mathrm{d}(r\ddot{f}_n^a)}{\mathrm{d}r} = \frac{\kappa}{r}(r\ddot{f}_n^a) - (\epsilon_n^a - V_0^a)(r\ddot{g}_n^a) - 2(r\dot{g}_n^a). \tag{34}$$

Now, we use the Bloch's sums of the functions R_3^{an}

$$\Phi_B^{an}(\boldsymbol{k}, \boldsymbol{r}) = \sum_{\boldsymbol{R}} \mathrm{e}^{\mathrm{i}\boldsymbol{k}\boldsymbol{R}} R_3^{an}(\boldsymbol{r}_a), \tag{35}$$

as the basis functions of the second type. Here $\boldsymbol{R}$ are the lattice vectors and $\boldsymbol{r}_a$ designates the radius vector measured from the centre of atom a: $\boldsymbol{r}_a = \boldsymbol{r} - \boldsymbol{t}_a$.

Finally, we can write down a solution of the Dirac–Kohn–Sham equation (7) as the linear combination of the basis functions of the first and second types:

$$\Psi_\lambda(\boldsymbol{k}, \boldsymbol{r}) = \sum_{Gs} A_\lambda^{Gs}(\boldsymbol{k}) \Phi_A(\boldsymbol{k} + \boldsymbol{G}, s; \boldsymbol{r}) + \sum_{an} B_\lambda^{an}(\boldsymbol{k}) \Phi_B^{an}(\boldsymbol{k}; \boldsymbol{r}). \tag{36}$$

The coefficients $A_\lambda^{Gs}(\boldsymbol{k})$ and $B_\lambda^{an}(\boldsymbol{k})$ should be determined variationally.

2.3. Matrix elements of the RSPFLAPW method

The variational problem, arising from the crystal Dirac equation (7), leads to the generalized eigenvalue problem

$$\begin{bmatrix} H_{AA} & H_{BA}^\dagger \\ H_{BA} & H_{BB} \end{bmatrix} \begin{vmatrix} A \\ B \end{vmatrix} = E \begin{bmatrix} O_{AA} & O_{BA}^\dagger \\ O_{BA} & O_{BB} \end{bmatrix} \begin{vmatrix} A \\ B \end{vmatrix} \tag{37}$$

where we have omitted indexes for brevity. The matrix elements O and H (overlap and Hamiltonian, respectively) may be decomposed into interstitial and sphere components, and the latter are further decomposed into spherical (kinetic energy plus the $l = 0$ part of the scalar potential) and non-spherical terms (plus the contribution from the magnetic field) in the case of the Hamiltonian.

The interstitial contribution exists for the functions of the first type only and is given by the following expressions.

Overlap:

$$O_{AA}^{Gs;G's'}(\boldsymbol{k})|_{\Omega_i} = \frac{N_{k+G} N_{k+G'}}{\Omega} \int_{\Omega_i} \mathrm{e}^{\mathrm{i}(G'-G)r} \, \mathrm{d}\boldsymbol{r} \left\{ \delta_{ss'} + \frac{c^2}{(c^2 + \epsilon_{k+G}^+)(c^2 + \epsilon_{k+G'}^+)} \right.$$
$$\left. \times [(\boldsymbol{k} + \boldsymbol{G}) \cdot (\boldsymbol{k} + \boldsymbol{G}')\delta_{ss'} + \mathrm{i}[(\boldsymbol{k} + \boldsymbol{G}) \times (\boldsymbol{k} + \boldsymbol{G}')] \cdot \langle u_s|\boldsymbol{\sigma}|u_{s'}\rangle] \right\}. \tag{38}$$

Kinetic energy:

$$(H_{kin})_{AA}^{Gs;G's'}(\boldsymbol{k})|_{\Omega_i} = \epsilon_{k+G'}^+ O_{11}^{Gs;G's'}(\boldsymbol{k})|_{\Omega_i}. \tag{39}$$

Scalar potential:

$$V_{AA}^{Gs;G's'}(\boldsymbol{k})|_{\Omega_i} = \frac{N_{k+G} N_{k+G'}}{\Omega} \int_{\Omega_i} V(r) \mathrm{e}^{\mathrm{i}(G'-G)r} \, \mathrm{d}\boldsymbol{r} \left\{ \delta_{ss'} + \frac{c^2}{(c^2 + \epsilon_{k+G}^+)(c^2 + \epsilon_{k+G'}^+)} \right.$$
$$\left. \times [(\boldsymbol{k} + \boldsymbol{G}) \cdot (\boldsymbol{k} + \boldsymbol{G}')\delta_{ss'} + \mathrm{i}[(\boldsymbol{k} + \boldsymbol{G}) \times (\boldsymbol{k} + \boldsymbol{G}')] \cdot \langle u_s|\boldsymbol{\sigma}|u_{s'}\rangle] \right\}. \tag{40}$$

Magnetic field:

$$
\begin{aligned}
B_{AA}^{Gs;G's'}(k)|_{\Omega_i} = {} & \frac{N_{k+G}N_{k+G'}}{\Omega} \int_{\Omega i} B(r)\mathrm{e}^{\mathrm{i}(G'-G)r} \, \mathrm{d}r \left\{ \boldsymbol{n}_B \cdot \langle u_s|\boldsymbol{\sigma}|u_{s'}\rangle \right. \\
& - \frac{c^2}{(c^2+\epsilon_{k+G}^+)(c^2+\epsilon_{k+G'}^+)}[(\boldsymbol{n}_B \cdot (\boldsymbol{k}+\boldsymbol{G}))((\boldsymbol{k}+\boldsymbol{G}') \cdot \langle u_s|\boldsymbol{\sigma}|u_{s'}\rangle) \\
& + (\boldsymbol{n}_B \cdot (\boldsymbol{k}+\boldsymbol{G}'))((\boldsymbol{k}+\boldsymbol{G}) \cdot \langle u_s|\boldsymbol{\sigma}|u_{s'}\rangle) \\
& \left. - ((\boldsymbol{k}+\boldsymbol{G}) \cdot (\boldsymbol{k}+\boldsymbol{G}'))(\boldsymbol{n}_B \cdot \langle u_s|\boldsymbol{\sigma}|u_{s'}\rangle) - \mathrm{i}\boldsymbol{n}_B \cdot [(\boldsymbol{k}+\boldsymbol{G}) \times (\boldsymbol{k}+\boldsymbol{G}')]\delta_{ss'}] \right\}.
\end{aligned}
\tag{41}
$$

Here $\boldsymbol{n}_B$ indicates the direction of magnetic field.

The contributions to the overlap matrix elements from the MT-spheres are calculated via the following expressions:

$$
\begin{aligned}
O_{AA}^{Gs;G's'}(k)|_{MT} = {} & \sum_a \sum_{il\mu;i'l'\mu'} \left\{ y_1^{*ail\mu}(\boldsymbol{k}+\boldsymbol{G},s)y_1^{ai'l'\mu'}(\boldsymbol{k}+\boldsymbol{G}',s') \right. \\
& \times \int_{\Omega_a} R_1^{\dagger ail\mu}(r)R_1^{ai'l'\mu'}(r) \, \mathrm{d}r + y_1^{*ail\mu}(\boldsymbol{k}+\boldsymbol{G},s)y_2^{ai'l'\mu'}(\boldsymbol{k}+\boldsymbol{G}',s') \\
& \times \int_{\Omega_a} R_1^{\dagger ail\mu}(r)R_2^{ai'l'\mu'}(r) \, \mathrm{d}r + y_2^{*ail\mu}(\boldsymbol{k}+\boldsymbol{G},s)y_1^{ai'l'\mu'}(\boldsymbol{k}+\boldsymbol{G}',s') \\
& \times \int_{\Omega_a} R_2^{\dagger ail\mu}(r)R_1^{ai'l'\mu'}(r) \, \mathrm{d}r + y_2^{*ail\mu}(\boldsymbol{k}+\boldsymbol{G},s)y_2^{ai'l'\mu'}(\boldsymbol{k}+\boldsymbol{G}',s') \\
& \left. \times \int_{\Omega_a} R_2^{\dagger ail\mu}(r)R_2^{ai'l'\mu'}(r) \, \mathrm{d}r \right\}
\end{aligned}
\tag{42}
$$

$$
\begin{aligned}
O_{BA}^{an;G's'}(k)|_{MT} = {} & \sum_{i'l'\mu'} \left\{ y_1^{ai'l'\mu'}(\boldsymbol{k}+\boldsymbol{G}',s') \int_{\Omega_a} R_3^{\dagger an}(r)R_1^{ai'l'\mu'}(r) \, \mathrm{d}r \right. \\
& \left. + y_2^{ai'l'\mu'}(\boldsymbol{k}+\boldsymbol{G}',s') \int_{\Omega_a} R_3^{\dagger an}(r)R_2^{ai'l'\mu'}(r) \, \mathrm{d}r \right\}
\end{aligned}
\tag{43}
$$

$$
O_{BB}^{a,nn'}|_{MT} = \int_{\Omega_a} R_3^{\dagger an}(r)R_3^{an'}(r) \, \mathrm{d}r.
\tag{44}
$$

The integrals in these formulae are calculated via the orthonormality property of the spin-angular functions (19). The contributions to the Hamiltonian matrix elements from the MT-spheres are calculated via the following expressions:

$$
\begin{aligned}
H_{AA}^{Gs;G's'}(k)|_{MT} = {} & \sum_a \sum_{il\mu;i'l'\mu'} \left\{ y_1^{*ail\mu}(\boldsymbol{k}+\boldsymbol{G},s)y_1^{ai'l'\mu'}(\boldsymbol{k}+\boldsymbol{G}',s') \right. \\
& \times \int_{\Omega_a} R_1^{\dagger ail\mu}(r)\hat{H} R_1^{ai'l'\mu'}(r) \, \mathrm{d}r + y_1^{*ail\mu}(\boldsymbol{k}+\boldsymbol{G},s)y_2^{ai'l'\mu'}(\boldsymbol{k}+\boldsymbol{G}',s') \\
& \times \int_{\Omega_a} R_1^{\dagger ail\mu}(r)\hat{H} R_2^{ai'l'\mu'}(r) \, \mathrm{d}r + y_2^{*ail\mu}(\boldsymbol{k}+\boldsymbol{G},s)y_1^{ai'l'\mu'}(\boldsymbol{k}+\boldsymbol{G}',s') \\
& \times \int_{\Omega_a} R_2^{\dagger ail\mu}(r)\hat{H} R_1^{ai'l'\mu'}(r) \, \mathrm{d}r + y_2^{*ail\mu}(\boldsymbol{k}+\boldsymbol{G},s)y_2^{ai'l'\mu'}(\boldsymbol{k}+\boldsymbol{G}',s') \\
& \left. \times \int_{\Omega_a} R_2^{\dagger ail\mu}(r)\hat{H} R_2^{ai'l'\mu'}(r) \, \mathrm{d}r \right\}
\end{aligned}
\tag{45}
$$

$$H_{BA}^{an;G's'}(\boldsymbol{k})|_{MT} = \sum_{i'l'\mu'} \left\{ y_1^{ai'l'\mu'}(\boldsymbol{k}+\boldsymbol{G}', s') \int_{\Omega_a} R_3^{\dagger an}(\boldsymbol{r}) \hat{H} R_1^{ai'l'\mu'}(\boldsymbol{r}) \, \mathrm{d}\boldsymbol{r} \right.$$

$$\left. + y_2^{ai'l'\mu'}(\boldsymbol{k}+\boldsymbol{G}', s') \int_{\Omega_a} R_3^{\dagger an}(\boldsymbol{r}) \hat{H} R_2^{ai'l'\mu'}(\boldsymbol{r}) \, \mathrm{d}\boldsymbol{r} \right\} \tag{46}$$

$$H_{BB}^{a,nn'}|_{MT} = \int_{\Omega_a} R_3^{\dagger an}(\boldsymbol{r}) \hat{H} R_3^{an'}(\boldsymbol{r}) \, \mathrm{d}\boldsymbol{r}. \tag{47}$$

In these formulae, the integrals of $\hat{H}_{kin} + V_0$ are calculated via (14), (15), (32) and with the orthonormality property of spin-angular functions (19). The integrals for the non-spherical part of the scalar potential and the magnetic field are evaluated by using the representations

$$V(\boldsymbol{r}) = \sum_{lm} V_{lm}(r) Y_{lm}(\hat{\boldsymbol{r}}) \tag{48}$$

$$\boldsymbol{B}(\boldsymbol{r}) = \sum_{lm} B_{lm}(r) Y_{lm}(\hat{\boldsymbol{r}}) \tag{49}$$

and (17).

It is necessary to note that spin-polarization is treated by perturbation in our code, and not on an equal footing with spin–orbit coupling. We believe, however, that utilization of LO relaxes this approximation.

2.4. Orbital and spin magnetic moments

Knowledge of the wavefunctions $\Psi_\lambda(\boldsymbol{k}, \boldsymbol{r})$ allows us to calculate an orbital magnetic moment for each of the atoms as

$$\boldsymbol{\mu}_{orb}^a = \sum_{\boldsymbol{k}} \sum_\lambda \int_{\Omega_a} \mathrm{d}\boldsymbol{r} \, \Psi_\lambda^\dagger(\boldsymbol{k}, \boldsymbol{r}) \beta \hat{\boldsymbol{l}} \Psi_\lambda(\boldsymbol{k}, \boldsymbol{r}) \theta[E_F - E_\lambda(\boldsymbol{k})]. \tag{50}$$

The magnetic spin moment can be calculated as an integral of the magnetization density (5) over MT-sphere of atom a:

$$\boldsymbol{\mu}_{spin}^a = \int_{\Omega_a} \boldsymbol{m} \, \mathrm{d}\boldsymbol{r}. \tag{51}$$

2.5. Short discussion of the code, optimization and parallelization strategy

The computer code we developed has two principal parts: non-relativistic (scalar-relativistic) and fully relativistic. They have been written as one code because only a few things are different for the two parts: the radial equations, the construction of the matrix elements, and the calculation of the electronic (magnetization) density. Apart from these two options there are also other possibilities: LDA or GGA for the exchange and correlation energy, non-spin-polarized or spin-polarized calculations, different schemes of mixing of the charge density in the course of self-consistency, and the automatic calculation of elastic constants for all types of lattices.

The LAPW method has relatively high requirements for computer hardware, and the calculations performed with it take much time. That is why we have written the code in such a way that the bulk of the calculations is performed by utilizing well known basic linear algebra subprograms (BLAS), as is also done in the WIEN-97 code [36].

We have also applied parallelization to the most time consuming parts of the code. Our parallelization strategy is very close to that described in [37], so we do not give any details here.

Table 1. Comparison of the ground state properties of light actinides (in the fcc structure) obtained in [13] by the methods LCGTO-FF and FLAPW with those, obtained with the scalar-relativistic part of the code presented here.

Method	Equilibrium volume (au)	Bulk modulus (GPa)
Th		
LCGTO-FF	216.9	58.8
FLAPW	219.3	56.7
FLAPW, present work	217.4	57.1
Pa		
LCGTO-FF	171.5	102
FLAPW	172.3	100
FLAPW, present work	171.4	94.8
U		
LCGTO-FF	146.1	101
FLAPW	147.5	125
FLAPW, present work	147.3	117
Np		
LCGTO-FF	131.6	142
FLAPW	131.4	137
FLAPW, present work	130.7	137
Pu		
LCGTO-FF	121.2	170
FLAPW	122.3	153
FLAPW, present work	119.8	156

Because we present a new code, it is interesting to do some comparisons with existing calculations in which the same approach was used. In table 1 we have collected the ground state properties of the light actinides (in the fcc structure) as obtained by two full-potential methods [13]: the linear combinations of the Gaussian-type orbitals-fitting function (LCGTO-FF) method, and the full-potential linearized augmented plane-wave (FLAPW) method in scalar-relativistic approximation and without spin-polarization. The results obtained with the our code are also presented in the table 1.

As can be seen, our results for the ground state properties are close to those obtained in [13], although small differences exist. We believe that they are due to the different methods of BZ integrations: all BZ integrations were reduced to simple sums of a Fermi–Dirac-function integrand in [13] with 60 irreducible points, whereas we used a tetrahedron method [38] with 195 irreducible points in BZ. We have also compared (table 4) our ground state properties for α-Pu (obtained with non-spin-polarized calculations and with the scalar-relativistic approach) with the corresponding properties obtained by another FLAPW code in [13]. Agreement is very close.

The following test has been performed to assess the quality of calculating the spin–orbit interaction. As is well known, there are some problems with the diagonalization of the Dirac Hamiltonian within a finite scalar-relativistic basis [39]. As has been shown in [39] for the fcc-Th, this manifests itself in a sensitivity of the calculated total energy to the value chosen for the muffin-tin radius. Therefore we have carried out RFLAPW total-energy calculations as a function of volume for the fcc-Th in the same manner as that carried out in [39], for
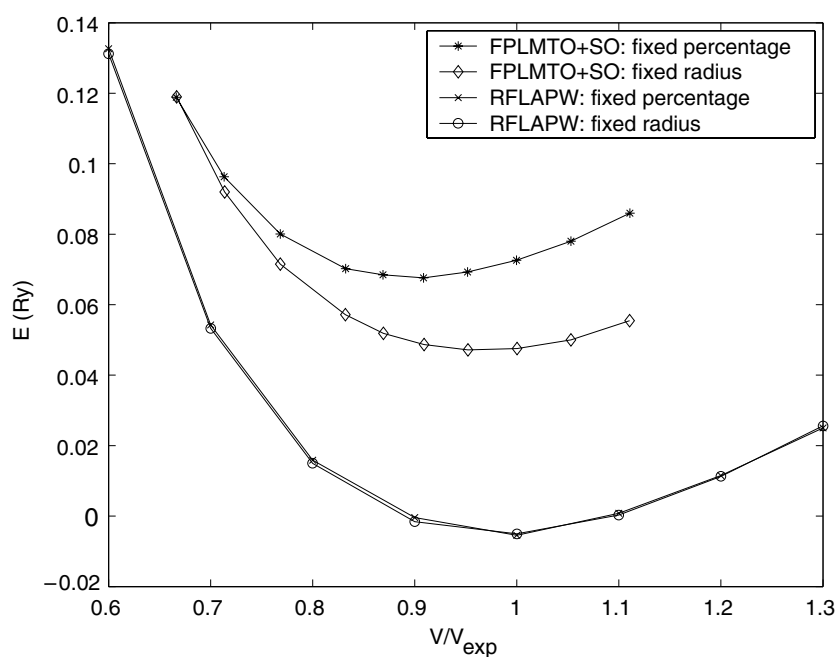
Figure 1. Calculated total energy of Th for fixed muffin-tin volume and for the muffin-tin volume being a fixed fraction of the unit cell volume. The zeros of energy for the results, obtained by the FP-LMTO method [39] and by our RFLAPW method are shifted arbitrarily for convenience.

two different choices of the muffin-tin radius: one using a constant muffin-tin volume for all calculated volume/energy points, and the other using a constant ratio between the muffin-tin volume and unit cell volume, for all calculated points. In figure 1 we show our results together with those from [39].

As can be seen from figure 1, a dependence on the value of the MT-radius is practically absent in the case of RFLAPW, and the equilibrium volume obtained is very close to the experimental equilibrium volume (the calculated 0 K equilibrium volume and bulk modulus are, respectively, 217.7 au and 59.9 GPa versus experimental 300 K values of 221.7 au and 58 GPa [13]). Thus, the choice of the muffin-tin radius or the constant ratio of muffin-tin volume to cell volume is not so important for the present fully relativistic method. This is in contrast to other methods, which use the variational treatment of the spin–orbit interaction in the scalar-relativistic basis.

3. Parameters and results of calculations

Here, we present results for two phases of plutonium, the α and the δ phases. The ferromagnetic (FM), AFM and NM structures were considered. The AFM δ-Pu case was treated similar to that in [14] and [20], i.e. a tetragonal lattice unit cell which includes two atoms at (0, 0, 0) and (1/2, 1/2, 1/2) was used. The FM consideration of α-Pu means that the atoms, connected by symmetry transformations (equivalent atoms) have initially equal spin moments and equal orbital moments. The final result obtained in the course of self-consistency indeed shows alignment of the moments in a ferrimagnetic structure, because there are sublattices with different directions of moments. The AFM consideration of α-Pu means that equivalent atoms

have the opposite directions of moments. Thus, in the AFM case, the cell sum of the atomic moments is always equal to zero.

Because the fully relativistic calculations of α-Pu are very time consuming, they were performed at experimental equilibrium volume only, and the geometry optimization was not carried out. The lattice parameters and the coordinates of the atoms in the unit cell were taken from [40].

The radii of the muffin-tin spheres were assumed to be identical for all the structures and they have been taken to be equal to the radii of the almost touching spheres in the structure of α-Pu. The constant ratio of the muffin-tin volume to the cell volume was kept the same at all volumes studied.

Within the muffin-tin spheres the charge density and potential were expanded in spherical harmonics with a cutoff L_{max} equal to 6. The angular momentum cutoff $L_{max} = 8$ was used for the basis functions. The basis set also included the semicore orbitals 5d, 6s and 6p. The plane wave expansion of the wavefunctions was terminated in such a manner that the total energy converged to better than 1 mRyd/atom. The density and the potential in the interstitial were represented by a Fourier series consisting of 14 383, 6615, and 35 983 plane waves for fcc (AFM), fcc (FM), and α-Pu structures, respectively.

The integration over BZ was carried out by the improved tetrahedron method [38]. For the FM-fcc calculations we used up to 480 points in the irreducible part of the BZ. For the AFM-fcc calculations we used 456 irreducible points. Thirty irreducible points were used for α-Pu calculations.

3.1. Structural stability

First of all, the relative stability of the different magnetic structures of α-Pu and δ-Pu was investigated (figure 2). As can be seen, the energy of the AFM structure of δ-Pu is below the energies of the FM or NM structures of this phase, as it has already been stated in [14] and [20]. Further, fully relativistic calculations enhance the stability of α-Pu. This is possibly a consequence of an enhanced bonding in this phase (relativistic treatment of the interstitial region is more important in this case).

An important observation from figure 2 is that the AFM and ferrimagnetic structures of α-Pu have almost the same energies in the fully relativistic calculation with the energy of the AFM phase lying about 0.5 mRyd lower. This difference is less in fully relativistic calculations than in scalar-relativistic ones. Thus, the fully relativistic treatment is more consistent with the concept of many magnetic configurations with almost equal energies (see conclusions).

3.2. Magnetic structure

In figure 3, both the spin and the orbital magnetic moments of each atom in α-Pu for both FM and AFM calculations are presented.

Both the AFM phase and the ferrimagnetic phase have sublattices with different directions of magnetic moments. The total moment of the unit cell is exactly equal to zero in the AFM structure and it is almost equal to zero in the ferrimagnetic case (see table 2). Obviously, the conclusion from our present work on magnetic properties of the ground state of plutonium coincides with the conclusion reached in [7]. As one can see from figure 3, the orbital moments are always directed opposite to the spin moments. Thus, there is a tendency to cancellation of the spin and orbital magnetic moments, and this fact may lead to a temperature independent magnetic susceptibility of α-Pu via a very large Van Vleck contribution.

The values of spin and orbital magnetic moments have been collected in table 2. The numbering of the atoms in this table for the α-Pu structure corresponds to the numbering
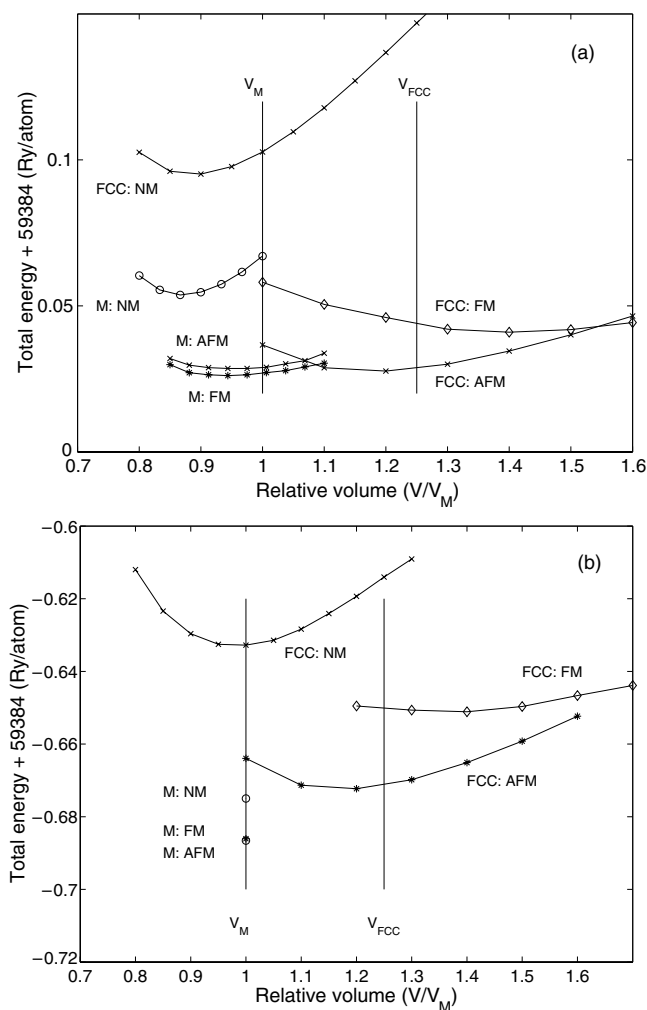
Figure 2. Total energy of α-Pu (M, monoclinic) and δ-Pu (FCC) from scalar-relativistic (a) and fully relativistic (b) calculations. The two vertical lines represent experimental equilibrium volumes for α-Pu (V_M) and (V_{FCC}).

accepted in [40]. As is apparent, the magnetic moments of fcc-plutonium are larger than those of α-Pu. This is a consequence of the stronger localization of the 5f states in δ-Pu.

It is necessary to note that, as is clear from relations (50) and (51), the values of the orbital and spin magnetic moments are dependent of the muffin-tin radius. However this dependence is not so strong. Indeed, decreasing the MT-sphere's volumes by 25% (at the same volume of the unit cell) in δ-Pu gives only a 2.5% decrease in the magnetic moments.

Our result on the stability of the magnetic structure for α-Pu is contrary to the work of Söderlind [20], who found α-Pu to be non-magnetic. We think that this is due to the difference in the BZ integrations: we have used a tetrahedron method [38] whereas Söderlind used a method of special k-points with a Gaussian broadening of each energy eigenvalue. This broadening might be responsible for the suppression of the moments. This might also be a reason for the very difficult convergence of magnetic moments in the case of α-Pu, as stated in [11]. It is unlikely, however, that the different treatment of spin–orbit interaction could
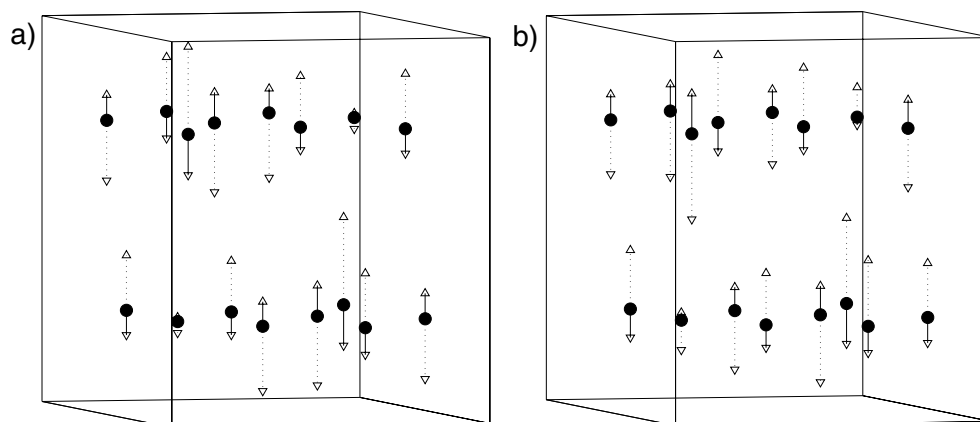
Figure 3. The magnetic structure of α-Pu at the experimental equilibrium volume obtained from relativistic calculations ((a) FM ordering of the moments, (b) AFM ordering). Solid arrows, orbital moments. Dashed arrows, spin moments. Magnetic moments are given in arbitrary units (the maximum spin moment among the atoms is approximately 3.5 μ_B (see table 2)).

Table 2. The atomic magnetic moments (in Bohr's magnetons) of plutonium as obtained from relativistic calculations. All values are from calculations at experimental equilibrium volumes: 20 Å^3/atom for α-Pu and 25 Å^3/atom for δ-Pu.

		FM			AFM		
Structure	Atom	S	L	Total	S	L	Total
α-Pu	1	−0.46	0.18	−0.28	−1.21	0.31	−0.90
	2	2.22	−1.00	1.22	2.39	−1.16	1.23
	3	−2.62	0.99	−1.63	2.10	−0.94	1.16
	4	2.07	−0.94	1.13	−2.39	0.96	−1.43
	5	2.20	−1.09	1.11	2.67	−1.08	1.59
	6	−2.80	1.24	−1.56	−2.74	1.17	−1.57
	7	−2.44	1.03	−1.41	2.20	−1.04	1.16
	8	3.54	−1.65	1.89	3.47	−1.64	1.83
	Average moment	0.21	−0.16	0.05	0.00	0.00	0.00
δ-Pu	1				4.09	−1.75	2.34
	Average moment				0.00	0.00	0.00

be the reason for the discrepancy, because the magnetic moments were also formed in our scalar-relativistic calculations.

3.3. Electronic structure

We have also studied the effect of spin-polarization on the density of states (DOS) for both α-Pu and δ-Pu. DOS, in principle, can be compared with experimental photoelectron spectra (PES), although with some disclaimers. For comparison, we show in figure 4 our calculated DOS for δ-Pu and α-Pu together with PES data from [41]. The DOS obtained by Penicaud [17] for NM α-Pu is also shown for comparison. The difference between our calculation and Penicaud's is in the different treatment of spin–orbit interaction, and Penicaud's DOS have also been convoluted with a Gaussian function of width 0.05 eV. It is clear that the two DOS are very close to each other if one takes into consideration this convolution.
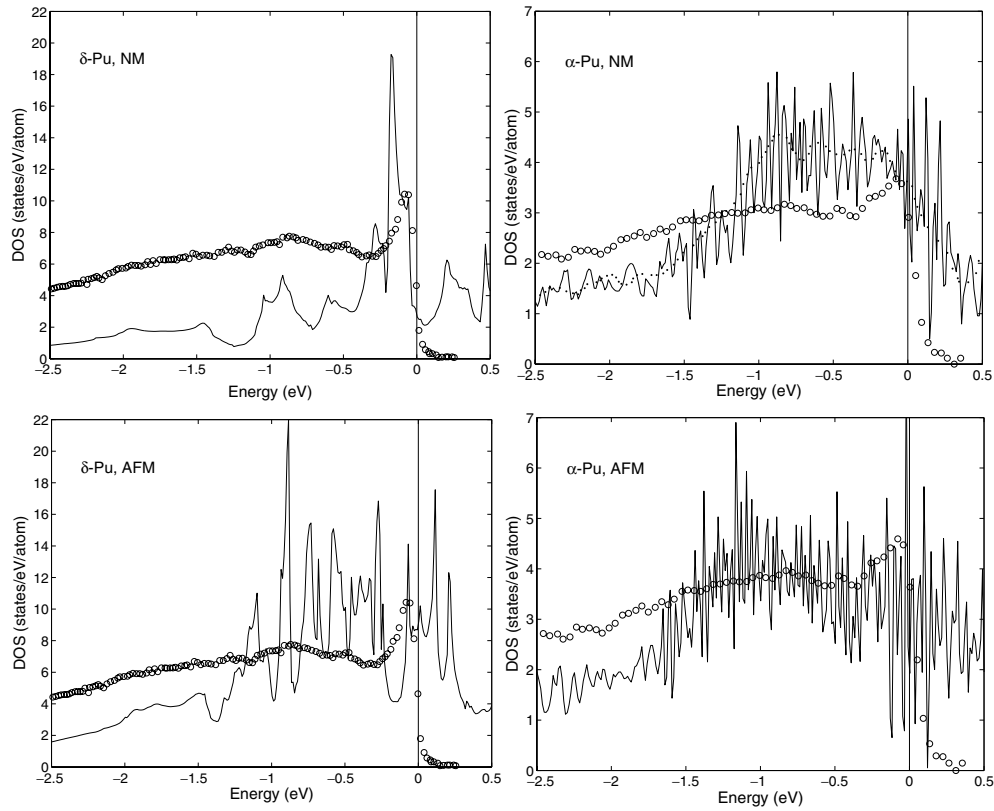
Figure 4. Comparison of the calculated DOS (solid curves) with the experimental PES (circles) [41]. All the calculations are fully relativistic here. The experimental intensities are given in arbitrary units. The dotted curve in top right figure is the calculated DOS from [17]. DOS has been calculated at atomic volumes 25.0 Å^3 for δ-Pu and at 20.0 Å^3 for α-Pu. NM, non-spin-polarized calculation; AFM, spin-polarized calculation with AFM order. Energies are relative to the Fermi energy.

As can be seen from figure 4, the DOS of δ-Pu obtained from non-spin-polarized calculations show no 5f peak at E_f, and its behaviour is qualitatively different from the PES measurements. The same is true for α-Pu: the peak of the DOS just below the Fermi energy is not presented in the non-spin-polarized calculation. DOS from spin-polarized calculations are much closer to the PES spectra for both δ-Pu and α-Pu. This observation has already been made by Söderlind *et al* for δ-Pu [22]. Hence, our result also provides further evidence for magnetic interactions in α-Pu.

3.4. Ground state properties

We have also computed the ground state properties of α-Pu (in the scalar-relativistic approximation only) and δ-Pu. The ground state properties of δ-Pu as obtained in our relativistic calculations have been collected in table 3 together with those from other theoretical studies and from experiments. It is seen that careful treatment of the magnetic structure of fcc plutonium allows us to improve considerably the calculated ground state properties of this phase. It is noteworthy that this result was obtained without using the orbital polarization as was done in [20].

Table 3. The ground state properties of δ-Pu. (FPLMTO; RFLAPW; SO, taking the spin–orbit interaction into account as a variational step; OP, taking the orbital polarization into account).

Reference	Method	V_0 (au)	B_0 (Gpa)
[20]	FPLMTO, SO, GGA, OP (AFM)	172.8	35.8
[20]	FPLMTO, SO, GGA (FM)	182.2	21.0
[20]	FPLMTO, SO, GGA (NM)	134.3	102.5
[18]	FPLMTO, SO, LDA + U (FM)	170.1	61.0
[14]	FLAPW, $650K$	168.5	43.0
Present work	RFLAPW, GGA (NM)	132.7	90.7
Present work	RFLAPW, GGA (FM)	186.4	25.1
Present work	RFLAPW, GGA (AFM)	157.6	51.0
[42]	Experiment	168.7	29.9–35.0

Table 4. The ground state properties of α-Pu. SO means taking the spin–orbit interaction as a variational step; NM, non-spin-polarized calculation; FM, spin-polarized calculation (ferrimagnetic configuration); AFM, spin-polarized calculation (AFM configuration). All the calculations have been performed using GGA.

Reference	Method	V_0 (au)	B_0 (Gpa)
[11]	FPLMTO, SO, (NM)	124.2	130
[13]	FLAPW, (NM)	117.2	232
[13]	FLAPW, SO, (NM)	124.4	153
[21]	FLAPW, SO, (NM)	118.9	
Present work	FLAPW, (NM)	116.6	227
Present work	FLAPW, (FM)	125.2	69.6
Present work	FLAPW, (AFM)	128.2	62.6
[43]	Experiment	134.95	
[44]	Experiment		47.2
[45]	Experiment		54.6

Table 4 contains the ground state properties of α-Pu. As can be seen from table 4, the agreement with experimental data is improved when spin-polarization is included. This result may also serve as evidence for the importance of magnetic interactions in α-Pu. It is necessary to recall, however, that this result did not include spin–orbit interaction. We hope to do this in the near future.

4. Conclusions

In conclusion, we have obtained similar results for δ-Pu as the authors of earlier works [14, 20]. The fully relativistic calculations did not change the conclusions [14, 20] about AFM ordering of the moments in this phase of plutonium at low temperatures. However, δ-Pu is not stable at low temperatures. To describe quantitatively some thermal properties of it, it is necessary to take into consideration correlation effects together with lattice vibrations.

Some results on α-Pu obtained in our work and the experimental information cited in the introduction, allow us to propose the following model for this phase of plutonium. There are many configurations (generally speaking with magnetic order) in the electronic system of α-Pu, which have almost equal energies. These configurations are characterized by different directions of magnetic moments in the atoms. When the temperature increases the system fluctuates between them in such a manner that the magnetic moments of the atoms are equal to zero on average. This hypothesis explains both the anomalous temperature dependence of

electrical resistance and the temperature independent magnetic susceptibility. It is not clear, however, if any particular magnetically ordered configuration is stabilized at $T = 0$ K, or if the ground state at $T = 0$ K corresponds to a NM linear combination of magnetic configurations. In this regard, the DMFT looks very promising, because it is well suited for the description of fluctuating f-electrons. DFT is a one-particle theory, and one may not answer this question definitively with it, because there can only be one of the configurations in the calculation. However, calculations within DFT allow us to say whether this configuration is magnetic or not, and in our work we have found that α-Pu has AFM configuration. It is quite possible that the volume dependence of the energy for the configuration presented in spin-polarized DFT is close to the volume dependence of the true ground state energy of the system. If this is so, the good prediction for the bulk modulus in our spin-polarized scalar-relativistic calculations finds an explanation.

The theory that will completely explain the rather anomalous properties of plutonium and, in particular, its very complex phase diagram, must in the end be a many-particle theory. DMFT [19, 46] is a good candidate for such a theory. DMFT offers much greater possibilities for studying the crystal's properties (excitation spectra, direct access to finite temperatures) than do LDA or GGA. It is necessary to say, however, that the calculations performed within this method so far contain some simplifications (in particular, the semi-empirical parameter U is used) [19]. This is why these calculations are not fully *ab initio* yet, and more work is required to improve upon this approach.

Acknowledgments

References

[1] Wallace D C 1998 *Phys. Rev.* B **58** 15433
[2] Skriver H L, Andersen O K and Johansson B 1978 *Phys. Rev. Lett.* **41** 42
[3] Söderlind P, Nordstrom L, Yongming L and Johansson B 1990 *Phys. Rev.* B **42** 4544
[4] Solovyev I V, Liechtenstein A I, Gubanov V A, Antropov V P and Andersen O K 1991 *Phys. Rev.* B **43** 14414
[5] van Ek J, Sterne P A and Gonis A 1993 *Phys. Rev.* B **48** 16280
[6] Söderlind P, Eriksson O, Johansson B and Wills J M 1994 *Phys. Rev.* B **50** 7291
[7] Antropov V P, van Schilfgaarde M and Harmon B N 1995 *J. Magn. Magn. Mater.* **144** 1355
[8] Vitos L, Kollar J and Skriver H L 1997 *Phys. Rev.* B **55** 4947
[9] Penicaud M 1997 *J. Phys.: Condens. Matter* **9** 6341
[10] Söderlind P, Wills J M, Johansson B and Eriksson O 1997 *Phys. Rev.* B **55** 1997
[11] Söderlind P 1998 *Adv. Phys.* **47** 959
[12] Savrasov S Y and Kotliar G 2000 *Phys. Rev. Lett.* **84** 3670
[13] Jones M D, Boettger J C, Albers R C and Singh D J 2000 *Phys. Rev.* B **61** 4644
[14] Wang Y and Sun Y 2000 *J. Phys.: Condens. Matter* **12** L311
[15] Baskes M I 2000 *Phys. Rev.* B **62** 15532
[16] Fernando G W, Sevilla E H and Cooper B R 2000 *Phys. Rev.* B **61** 12562
[17] Penicaud M 2000 *J. Phys.: Condens. Matter* **12** 5819
[18] Bouchet J, Siberchicot B, Jollet F and Pasturel A 2000 *J. Phys.: Condens. Matter* **12** 1723
[19] Savrasov S Y, Kotliar G and Abrahams E 2001 *Nature* **410** 793
[20] Söderlind P 2001 *Europhys. Lett.* **55** 525
[21] Penicaud M 2002 *J. Phys.: Condens. Matter* **14** 3575
[22] Söderlind P, Landa A and Sadigh B 2002 *Phys. Rev.* B **66** 205109

[23] Meot-Reymond S and Fournier J M 1996 *J. Alloys Compounds* **232** 119
[24] Olsen C E and Elliott R O 1965 *Phys. Rev.* A **139** 437
[25] Jullien R, Beal-Monod M T and Coqblin B 1974 *Phys. Rev.* B **9** 1441
[26] Boring A M and Smith J L 2000 *Los Alamos Sci.* **26** 42
[27] Perdew J P, Burke S and Ernzerhof M 1996 *Phys. Rev. Lett.* **77** 3865
[28] Singh D J 1994 *Planewaves, Pseudopotentials and the LAPW Method* (Boston, MA: Kluwer–Academic)
[29] Rajagopal A K and Callaway J 1973 *Phys. Rev.* B **7** 1912
[30] Rajagopal A K 1978 *J. Phys. C: Solid State Phys.* **11** L943
[31] MacDonald and Vosko S H 1979 *J. Phys. C: Solid State Phys.* **12** 2977
[32] Ramana M V and Rajagopal A K 1979 *J. Phys. C: Solid State Phys.* **12** L845
[33] Hohenberg P and Kohn W 1965 *Phys. Rev.* A **140** 1133
[34] Landau L D and Lifshiz E M 1989 *Kvantovaya Elektrodynamika* (Moscow: Nauka) (in Russian)
[35] Arfken G 1969 *Mathematical Methods for Physicists* (New York: Academic)
[36] Petersen M, Wagner F, Hufnagel L, Scheffler M, Blaha P and Schwarz K 2000 *Comput. Phys. Commun.* **126** 294
[37] Canning A, Mannstadt W and Freeman A J 2000 *Comput. Phys. Commun.* **130** 233
[38] Blochl P E, Jepsen O and Andersen O K 1994 *Phys. Rev.* B **49** 16223
[39] Nordstrom L, Wills J M, Andersson P H, Söderlind P and Eriksson O 2000 *Phys. Rev.* B **63** 035103
[40] Espinosa F J, Villella P, Lashley J C, Conradson S D, Cox L E, Martinez R, Martinez B, Morales L, Terry J and Pereyra R A 2001 *Phys. Rev.* B **63** 174111
[41] Arko A J, Jouce J J, Morales L, Wills J, Lashley J, Wastin F and Rebizant J 2000 *Phys. Rev.* B **62** 1773
[42] Merz M D, Hammer J H and Kjarmo H E 1976 *Plutonium and Other Actinides* ed H Blank and R Lindner (Amsterdam: North-Holland)
[43] Zachariasen W H and Ellinger F H 1963 *Acta Crystallogr.* **16** 777
[44] Roof R B 1981 *Advances in X-Ray Analysis* (New York: Plenum) p 22
[45] Bridgman P W 1959 *J. Appl. Phys.* **30** 214
[46] Georges A, Kotliar G, Krauth W and Rozenberg M J 1996 *Rev. Mod. Phys.* **68** 13